OSU

The Ohio State University

ADVANCED ADAPTIVE ANTENNA TECHNIQUES

R. J. Mayhan and R. T. Compton, Jr.

The Ohio State University

ElectroScience Laboratory

Department of Electrical Engineering
Columbus, Ohio 43212

Quarterly Report 712684-7

Contract N00019-80-C-0181

December 1980

Naval Air Systems Command
Washington, D.C. 20361

NOTICES

When Government drawings, specifications, or other data are used for any purpose other than in connection with a definitely related Government procurement operation, the United States Government thereby incurs no responsibility nor any obligation whatsoever, and the fact that the Government may have formulated, furnished, or in any way supplied the said drawings, specifications, or other data, is not to be regarded by implication or otherwise as in any manner licensing the holder or any other person or corporation, or conveying any rights or permission to manufacture, use, or sell any patented invention that may in any way be related thereto.

SECURITY CLASSIFICATION OF THIS PAGE (When Data Entered)

REPORT DOCUMENTATION PAGE	READ INSTRUCTIONS BEFORE COMPLETING FORM
1. REPORT NUMBER	2. GOVT ACCESSION NO. AD-A115155	3. RECIPIENT'S CATALOG NUMBER
4. TITLE (and Subtitle) ADVANCED ADAPTIVE ANTENNA TECHNIQUES	5. TYPE OF REPORT & PERIOD COVERED Quarterly Report
	6. PERFORMING ORG. REPORT NUMBER ESL 712684-7
7. AUTHOR(s) R. J. Mayhan R. T. Compton, Jr.	8. CONTRACT OR GRANT NUMBER(s)
9. PERFORMING ORGANIZATION NAME AND ADDRESS The Ohio State University ElectroScience Laboratory, Department of Electrical Engineering Columbus, Ohio 43212	10. PROGRAM ELEMENT, PROJECT, TASK AREA & WORK UNIT NUMBERS
11. CONTROLLING OFFICE NAME AND ADDRESS Naval Air Systems Command Washington, D. C. 20361	12. REPORT DATE December 1980
	13. NUMBER OF PAGES 15
14. MONITORING AGENCY NAME & ADDRESS(if different from Controlling Office)	15. SECURITY CLASS. (of this report) Unclassified
	15a. DECLASSIFICATION/DOWNGRADING SCHEDULE

16. DISTRIBUTION STATEMENT (of this Report)

APPROVED FOR PUBLIC RELEASE
DISTRIBUTION UNLIMITED

17. DISTRIBUTION STATEMENT (of the abstract entered in Block 20, if different from Report)

18. SUPPLEMENTARY NOTES

19. KEY WORDS (Continue on reverse side if necessary and identify by block number)

Adaptive arrays
Antennas
Interference
Communications

20. ABSTRACT (Continue on reverse side if necessary and identify by block number)

This report describes progress under Naval Air Systems Command Contract N00019-80-C-0181 during the third quarterly period. Research on advanced adaptive antenna techniques is summarized.

DD FORM 1 JAN 73 1473 EDITION OF 1 NOV 65 IS OBSOLETE

SECURITY CLASSIFICATION OF THIS PAGE (When Data Entered)

TABLE OF CONTENTS

I. INTRODUCTION

This report describes progress under Naval Air Systems Command Contract N00019-80-C-0181 during the third quarterly period. This contract involves adaptive array studies in two areas: (1) the effects of element patterns and signal polarization on adaptive array performance, and (2) the capability of pulsed and swept CW jamming against adaptive arrays. In addition, a monograph on adaptive arrays is being prepared under this contract.

During the third quarterly period, we have concentrated on the two research areas: the effects of element patterns, and the effectiveness of pulsed jamming against adaptive arrays. Progress in these two areas is described ~~below.~~

II. PROGRESS

1. The Effects of Element Patterns on Array Performance

During this quarter we have examined the performance of adaptive arrays using elements with adjacent, narrowbeam patterns ("multiple fan beam arrays"). The purpose was to compare the performance of such arrays to that of arrays with isotropic elements. Such a comparison is useful because multiple fan beam elements have often been suggested for use in adaptive arrays.

Our results show that performance is usually better with isotropic elements than with narrowbeam elements. The most important difference appears to be that fan beam arrays have poorer resolution capability with closely spaced signals than do arrays with isotropic elements.

Specifically, we have compared the output signal-to-interference-plus-noise ratio (SINR) performance of several fan beam arrays with that of comparable arrays using isotropic elements. The following

approach was taken. It was assumed that a given sector of space must be covered by the array. Signals may arrive from anywhere within this sector. The fan beam array was chosen so each element of the array had a narrowbeam pattern covering part of the sector. The individual beams were pointed in different directions within the sector, with the patterns crossing at their 3 dB points. The narrower the beamwidths of the element patterns, the more elements were required to cover the sector. The performance of each multiple beam array was compared to that of an array of isotropic elements having the same number of elements. Every element in the "isotropic" array was assumed to have a pattern constant over the sector of interest but zero outside this sector. The gain of each element pattern (narrowbeam or isotropic) was properly normalized. (I.e, with the element viewed as a transmitting antenna, the total power radiated by the element in all directions of space was set to the same value for every element pattern.) Such normalization is necessary to make the SINR comparison meaningful. Two types of patterns were used for the narrowbeam elements:

$$f_j(\theta) = a \frac{\sin\left[\frac{k(\theta-\theta_j)}{2}\right]}{\left[\frac{k(\theta-\theta_j)}{2}\right]}$$

and

$$f_j(\theta) = a \cos^m\left(\frac{\theta-\theta_j}{2}\right)$$

where $f_j(\theta)$ is the voltage response of the j^{th} element to a signal from angle θ, and θ_j is the direction of the beam maximum. k and m are constants used to control the beamwidth, and a is a gain constant normalized as discussed above. Arrays with up to 8 elements have been studied.

Typically we found that a multiple beam array and an isotropic array yield comparable SINR when the desired signal is far from the interference. When the two signals are close, however, the isotropic

array appears to have better performance. A typical set of curves illustrating this result is shown in Figure 1. This figure shows the

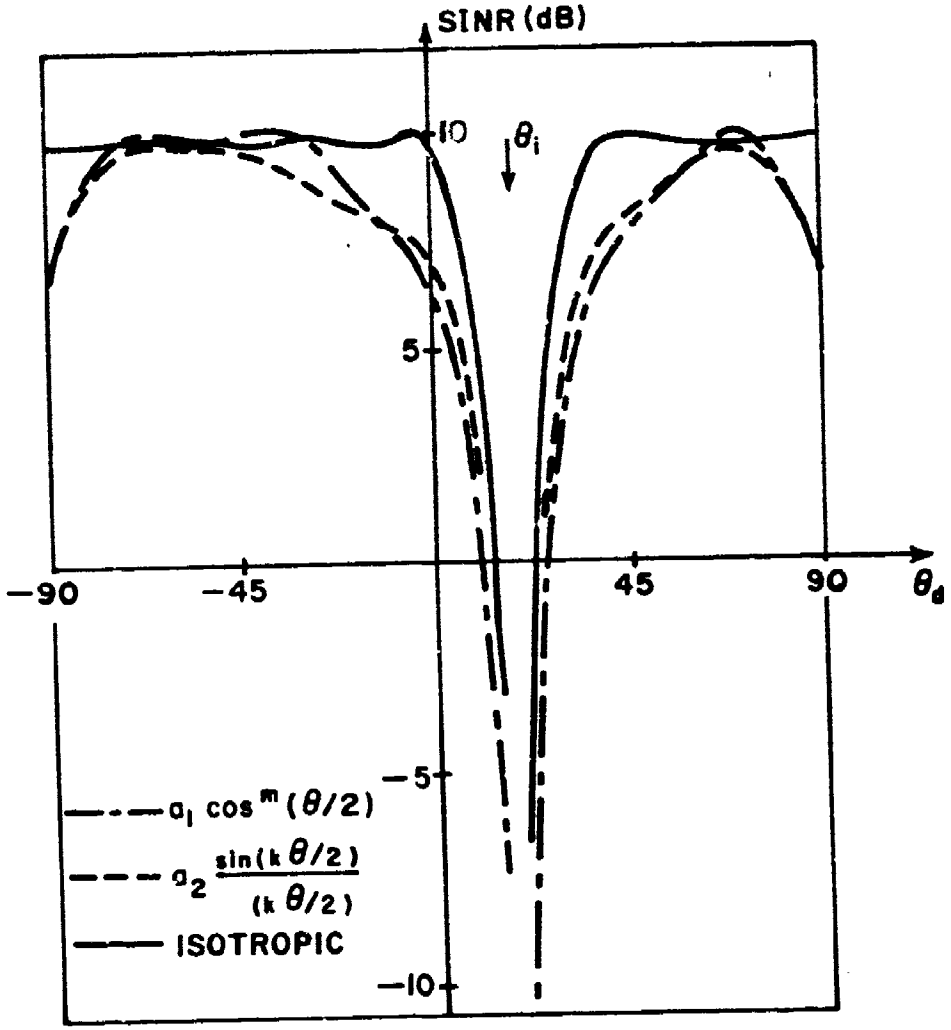

Figure 1. SINR (dB) vs. θ_d for a 5-element array.
Sector of coverage $-90^0 \leq \theta_d \leq 90^0$. $\theta_i = 18^0$
Isotropic array: $a^2 = 2$
Fan beam arrays: m=27.98; k=8.86;
look angles $\pm 72^0$, $\pm 36^0$, 0^0; $a_1^2 = 9.42$; $a_2^2 = 9.07$

SINR versus θ_d (the desired signal arrival angle) for a 5-element array with half wavelength spacing. A single interference signal arrives from $\theta_i = 18^0$. (Signal bandwidths are zero.) The most important difference seen in Figure 1 is the poorer resolution capability of either fan beam array, compared with the isotropic array, when $\theta_d \neq \theta_i$. This poorer resolution occurs with a fan beam array because elements far from the center of the array have a low response to both signals and hence add little resolving power to the array. A less important difference between the curves in Figure 1 is that the SINR drops near $\theta_d = \pm 90^0$ for the multiple beam arrays, but not for the isotropic array. This drop occurs because the two end beams are 3 dB below the isotropic element patterns at these angles.

In general, it appears to be better to choose the element patterns as nearly uniform as possible over the desired sector of space, rather than covering different parts of the sector with different elements.

2. The Effects of Pulse Jamming on an Adaptive Array

During this quarter we have investigated the effect of a pulse jammer on the performance of an adaptive array. This work has two purposes: to determine the degradation in array performance that occurs with pulsed jamming, and to determine how to choose the jammer parameters to make it most disruptive against an adaptive array.

For this study, we have considered a 3-element LMS array. The elements are isotropic and spaced a half wavelength apart at the signal frequency. The array is shown in Figure 2. We assume a CW desired signal incident on the array from angle θ_d and a jammer incident from angle θ_i. (θ is defined in Figure 2.) The jammer is assumed to be a pulse-modulated sinusoid as shown in Figure 3a. The jammer pulses repeat periodically with a pulse repetition period of T_r seconds and

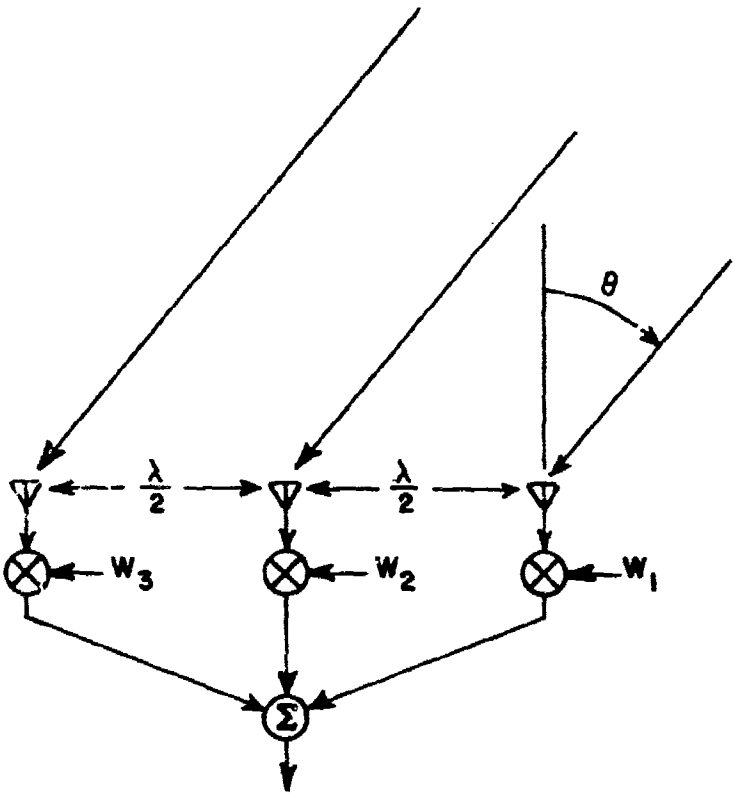

Figure 2. A 3-element adaptive array.

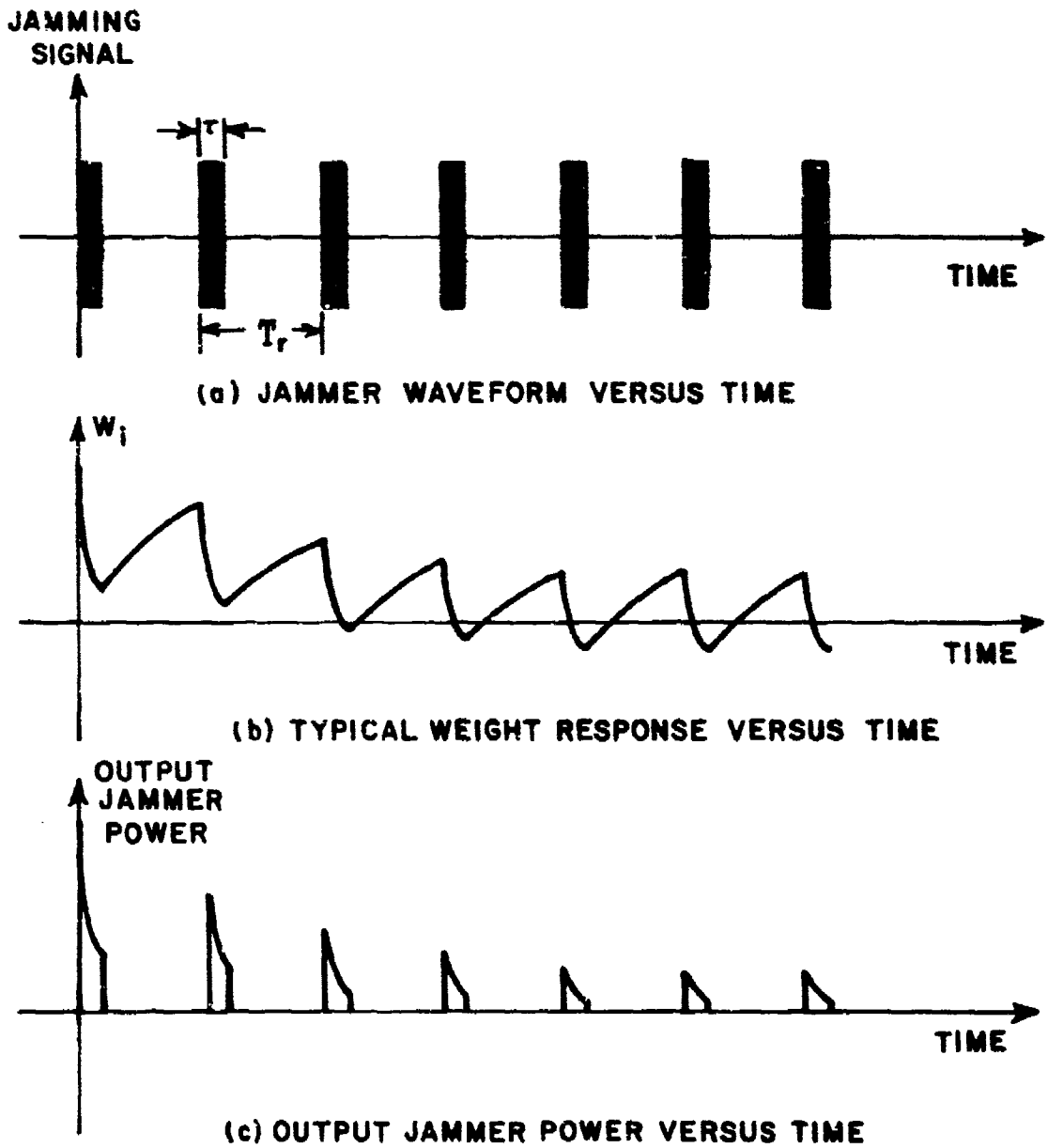

Figure 3. Jamming waveform and array response.

a pulse repetition frequency of $f_r = 1/T_r$ pulses per second. Each pulse has a duration of τ seconds, or equivalently, a duty cycle $\delta = \tau/T_r$. The center frequency of the interference is the same as that of the desired signal.

The effect of pulsed jamming is to cause the array weights to vary exponentially between two sets of values: those that would occur with a continuous jammer and those that would occur with no jamming. For large values of τ and T_r, compared to the array time constants, the array weights reach one set of steady-state values when the pulse is on and another when it is off. For very small values of τ and T_r, compared to the array time constants, the array weights are too slow to react during a pulse period and are essentially constant with time. For intermediate values of τ and T_r, however, the weights never reach steady-state. Instead, they vary exponentially back and forth. The pulse jammer does the most damage in this situation.

When a pulsed jammer signal first appears, the array weights start from the values they would have with only desired signal present. When the first pulse arrives, the array weights begin to change toward the values that a continuous jammer would produce. However, before the weights have reached steady-state, the interference turns off, so the weights then relax back toward their values for desired signal only. But before this second transient is finished, the next pulse arrives. Unless the pulse period is very large, the weights will not have the same initial values for the second pulse as they had for the first pulse. This behavior continues during the first few pulses, and results in weights transients that are different during each pulse. However, after a large number of pulses have arrived, the weights become periodic functions of time. They return to the same values at the end of each pulse repetition period as they had at the beginning of the period.

Figure 3 illustrates the initial transient behavior of the array when a pulsed jammer appears. Figure 3a shows the jammer pulses, Figure 3b the time response of a typical weight in the array, and Figure 3c the output jammer power from the array. The figure illustrates how the array weights and the output interference power settle into periodic waveforms after an initial transient interval.

In our work on pulsed jamming, we have concentrated on the performance of the array when the weights are in periodic steady-state, i.e., after the initial transients shown in Figure 3 have ended. Several computer programs have been developed to evaluate different aspects of the array performance. Programs have been developed that compute the amplitude and phase modulation on the desired signal, the jammer-to-noise ratio at the array output, and the output desired signal-to-jammer-plus-noise ratio, all as a function of time during the pulse period. Also, we have developed a program that computes the bit error probability as a function of the jammer parameters when the desired signal is a digital communication signal. These programs allow us to evaluate the effect of the desired signal and jammer arrival angles θ_d and θ_i, the desired signal-to-noise ratio (SNR), the jammer-to-noise ratio (INR), the pulse repetition period T_r, and the pulse length on the results.

Figures 4-13 illustrate typical results from these programs. Figure 4 shows the amplitude modulation produced on the desired signal by a pulsed jammer for the case $\theta_d = 0^o$, $\theta_i = 5^o$, $\tau/\tau_{min} = .01$, SNR = 10 dB, INR = 20 dB and $\tau_{min} f_r = 10$. ($\tau_{min} = 1/k\sigma^2$, where k is the LMS loop gain and σ^2 is the thermal noise power per element. τ_{min} is the slowest time constant in the array response and is a convenient parameter for normalizing τ and f_r.) The curve shows the instantaneous desired signal amplitude, normalized to the amplitude it would have in the absence of jamming, as a function of time t, over one period of the jammer. The values of τ and f_r given above yield a duty cycle of 1/10. During the period $0 \leq t \leq T_r/10$, the array is reacting to the jamming pulse.

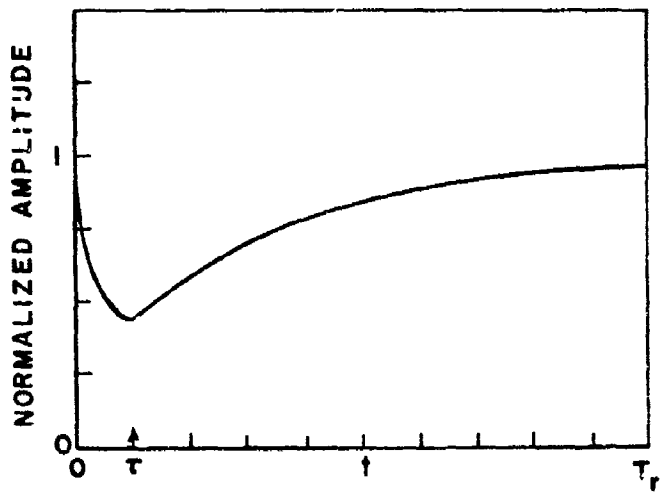

Figure 4. Desired signal amplitude modulation vs. time.
$\theta_d=0^0$, $\theta_j=5^0$, $k\sigma^2\tau=0.01$, $f_r/k\sigma^2=10$
SNR=10 dB, INR=20 dB

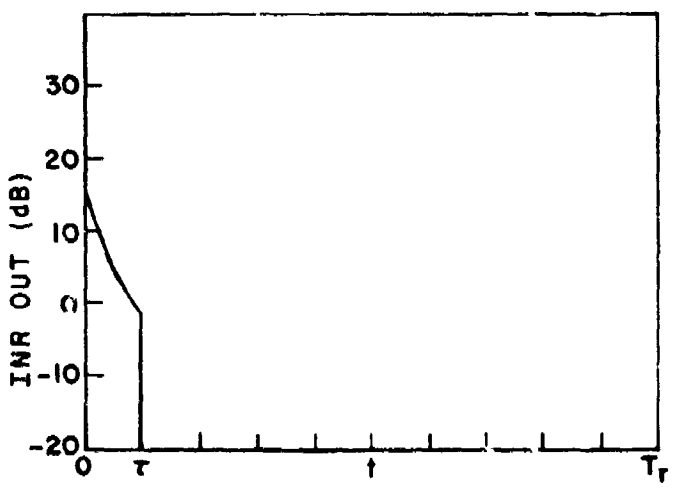

Figure 5. Output jammer-to-noise ratio (INR) vs. time.
$\theta_d=0^0$, $\theta_j=5^0$, $k\sigma^2\tau=0.01$, $f_r/k\sigma^2=10$,
SNR=10 dB, INR=20 dB

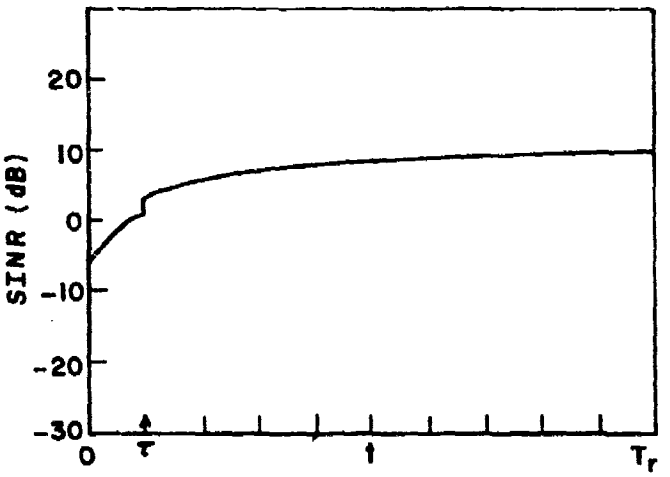

Figure 6. Output signal-to-jammer-plus-noise ratio (SINR) vs. time.
$\theta_d=0^0$, $\theta_j=5^0$, $k\sigma^2\tau=0.01$, $f_r/k\sigma^2=10$
SNR=10 dB, INR=20 dB

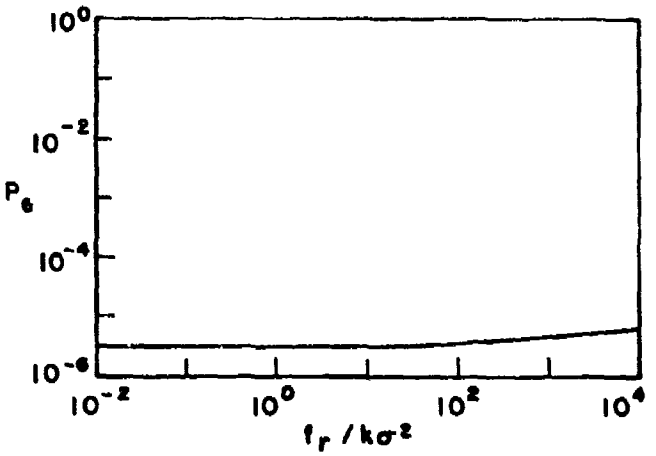

Figure 7. Bit error probability vs. PRF.
SNR=6 dB, INR=0 dB,
$\theta_d=0$, $\theta_j=60$, $k\sigma^2\tau = .0001$

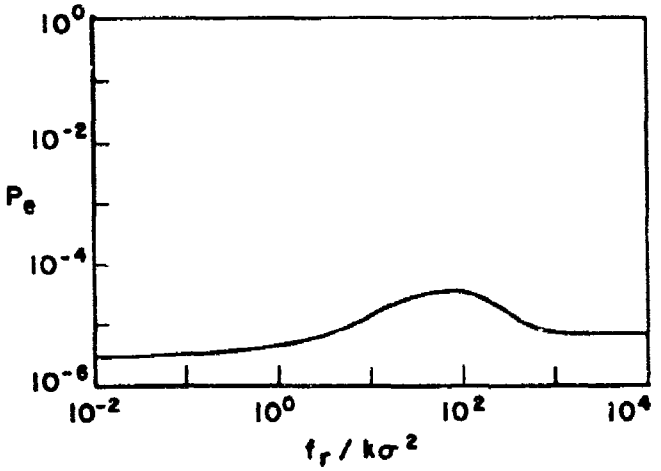

Figure 8. Bit error probability vs. PRF.
SNR=6 dB, INR=10 dB,
θ_d=0, θ_i=60, $k\sigma^2\tau$ =.0001

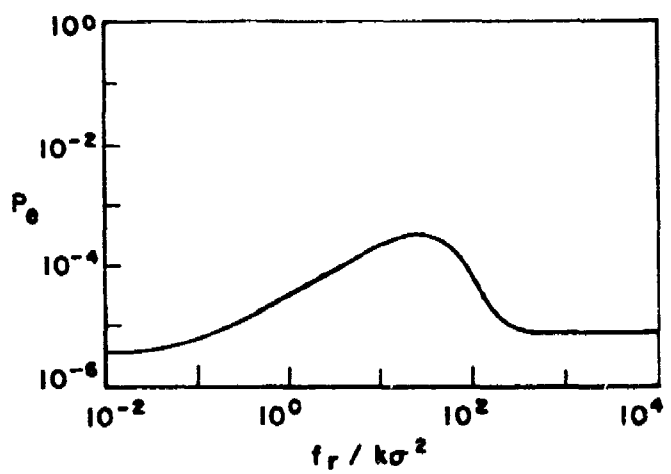

Figure 9. Bit error probability vs. PRF.
SNR=6 dB, INR=20 dB
θ_d=0, θ_i=60, $k\sigma^2\tau$ =.0001

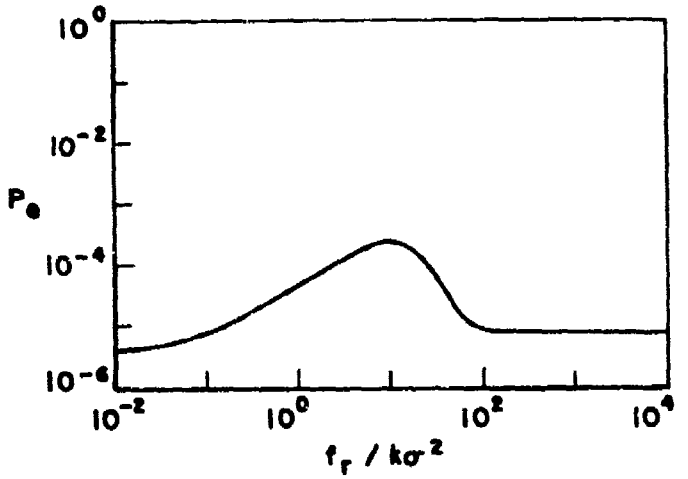

Figure 10. Bit error probability vs. PRF.
SNR=6 dB, INR=30 dB
θ_d=0, θ_j=60, $k\sigma^2\tau$ =.0001

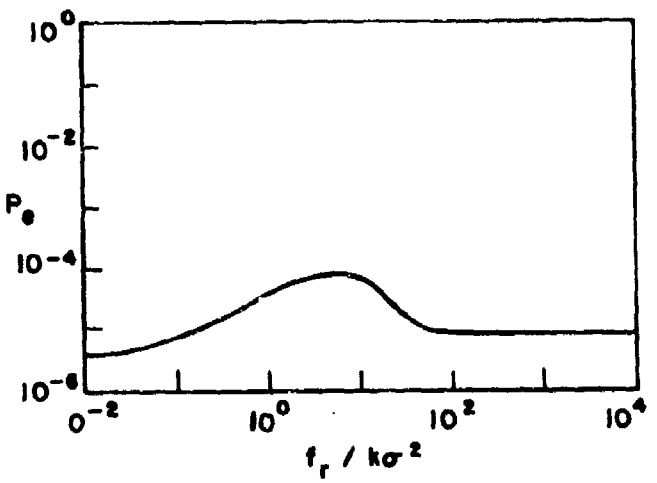

Figure 11. Bit error probability vs. PRF.
SNR=6 dB, INR=40 dB
θ_d=0, θ_j=60, $k\sigma^2\tau$ =.0001

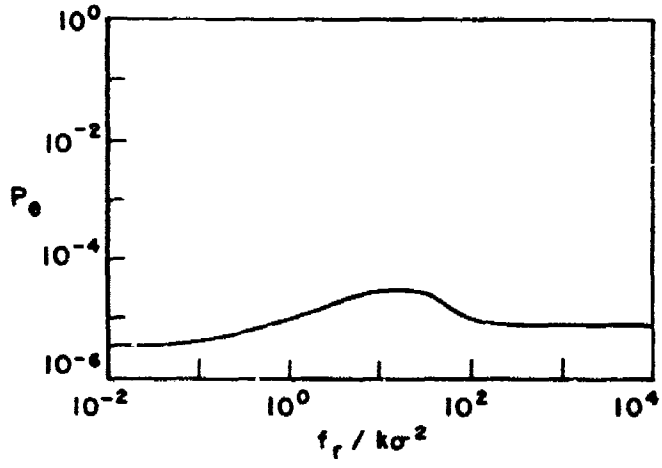

Figure 12. Bit error probability vs. PRF.
SNR=6 dB, INR=50 dB
θ_u=0, θ_j=60, $k\sigma^2\tau$ =.0001

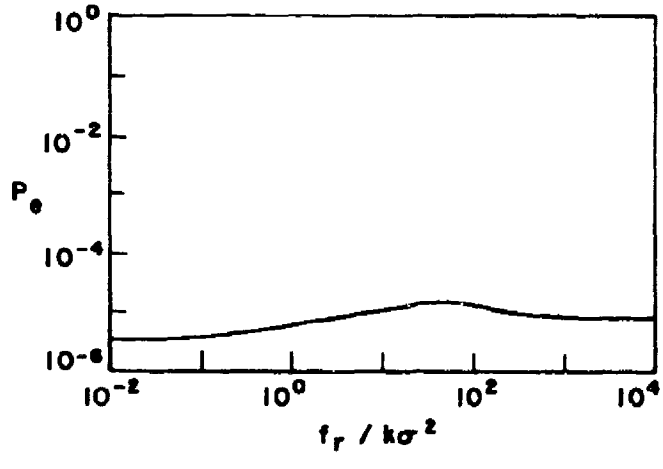

Figure 13. Bit error probability vs. PRF.
SNR=6 dB, INR=60 dB
θ_d=0, θ_j=60, $k\sigma^2\tau$ =.0001

During $T_r/10 \leq t \leq T_r$, the weights relax back toward the values they would have without jamming. It may be seen that the jammer produces substantial AM on the desired signal in this case.

Figure 5 shows the jammer-to-noise ratio (INR) at the array output, again as a function of time over the pulse repetition period, and for the same parameters as above. Since the jammer pulse is on only for $0 \leq t \leq T_r/10$, the output INR is nonzero only during this interval. It is seen how the array begins to null the jammer after it appears, but does not finish nulling it, before the pulse ends.

Figure 6 shows the desired signal-to-jammer-plus-noise ratio (SINR) at the array output during the pulse period, again for the same parameters. During the interval $0 \leq t \leq T_r/10$, the jamming power is present at the array output, so the SINR is low. At $t = T_r/10$, the SINR jumps up because the pulse disappears.

The curves shown in Figures 4-6 are all periodic functions. I.e., each curve repeats every pulse repetition period T_r.

Figures 7-13 show typical curves of bit error probability as a function of the jammer parameters. In these calculations, the desired signal is assumed to be a differentially-encoded, biphase-modulated (DPSK) communication signal. (Other desired signal modulations can be used in the program, but the results shown in Figures 7-13 are typical. Also, DPSK is a likely choice of modulation for use with an adaptive array.) Because of the pulsed jamming, a large number of bit errors occur when the pulse is on, but much fewer occur when the pulse is off. The bit error probabilities are computed by averaging the instantaneous bit error probability for each value of SINR over the jammer period. It is assumed in this calculation that the bit symbol duration is much shorter than the pulse length τ. The results in Figures 7-13 have been computed for SNR=6 dB, $\theta_d = 0^0$, $\theta_j = 60^0$ and $\tau/\tau_{min} = 0.0001$. Each

curve shows the bit error probability as a function of the (normalized) pulse repetition frequency of the jammer, over the range 10^{-2} to 10^{4}. The different figures are for different jammer powers. Figure 7 is for INR=0 dB, Figure 8 for INR=10 dB, and so forth, up to Figure 13 for INR=60 dB.

These curves are interesting for two reasons. First, they illustrate the nature of the optimization problem faced by the designer of the jammer. For this pulse width, it is seen that the INR must be in the range of 20 to 30 dB to increase the bit error probability significantly above its value with no jamming. I.e., if the jammer power is either too weak or too strong, the jammer will not be effective. In addition, the (normalized) pulse repetition frequency must be approximately 10 to optimize the jammer impact. Although it cannot be seen in these figures, it turns out that the optimum value of f_r also depends on the SNR, the INR, θ_d, θ_i and the pulse width τ. Thus, optimizing the jammer parameters is tricky, and involves parameters that will often be unknown in advance. Second, Figures 7-13 are also interesting because they show that even with optimum pulse jamming, the increase in bit error probability is not necessarily disastrous. For the parameters used in these calculations, for example, a communication link designed for a bit error probability of 5×10^{-6} will have an error rate of only about 5×10^{-4} in the presence of optimum pulse jamming.

The computer programs described above have been used to run a large number of curves for various situations. The curves we present here are intended only to illustrate the type of results being obtained. We are currently reducing these results into a systematic form for presentation.